Eur. Phys. J. E (2016) **39**: 132
DOI 10.1140/epje/i2016-16132-4

THE EUROPEAN PHYSICAL JOURNAL E

Regular Article

Microgravity in a thin film: How confinement kills gravity*

Fabrizio Croccolo[1,2,a] and Henri Bataller[1]

[1] Laboratoire des Fluides Complexes et leurs Réservoirs - UMR5150, Université de Pau et des Pays de l'Adour, 1 Allée du Parc Montaury 64600 Anglet, France
[2] Centre National d'Études Spatiales (CNES) 2, Place Maurice Quentin, 75001 Paris, France

Received 28 September 2016 and Received in final form 28 November 2016
Published online: 27 December 2016 –

Abstract. Fluctuations in the presence of concentration gradients are long-ranged and decay diffusively for small spatial scales. At larger scales fluctuations are influenced by gravity and confinement. The confinement in the direction of the concentration gradient couples to gravity generating a slowing down that ends up in a diffusion-like behavior of fluctuations of size comparable to the vertical extension of the sample. The resulting enhanced diffusion coefficient depends on the solutal Rayleigh number of the system. For small (in modulus) values of the solutal Rayleigh number the apparent diffusion coefficient tends towards the normal one and a simple diffusive behavior is obtained. This is quite similar to what happens in microgravity conditions when the solutal Rayleigh number is drastically reduced because of the reduction of g by about 6 orders of magnitude. Experiments are shown for positive and negative solutal Rayleigh numbers smaller (in modulus) than 1000. The effect of the confinement on the statics is also investigated. Comparison with microgravity data obtained through the GRADFLEX project is performed.

1 Introduction

A fluid subject to a vertical thermal gradient in the terrestrial gravitational field shows a density profile that can be either parallel or anti-parallel to gravity thus determining the stability of the system. A fluid heated from below is unstable provided the Rayleigh number $Ra_T = \beta_T \mathbf{g} \cdot \boldsymbol{\nabla} T L^4/(\nu\kappa)$ exceeds the critical value $Ra_{T,\mathrm{cr}} = 1708$ [1]. Here $\beta_T = \rho^{-1}(\partial\rho/\partial T)$ is the thermal expansion coefficient, ρ the fluid density, T the temperature, g the gravitational acceleration, $\boldsymbol{\nabla} T$ the temperature gradient, L the vertical extension of the sample, ν the kinematic viscosity and κ the thermal diffusivity. If the fluid consists of a mixture of two components the situation is more complex as the temperature gradient can induce separation of the species through the Soret effect and therefore the density profiles end up to be the sum of a temperature and a concentration profile. The picture is further complicated by the fact that the concentration profile can be parallel or anti-parallel to the temperature one depending on the sign of the Soret coefficient $S_T = -\Delta c/[c_o(1-c_o)\Delta T]$, where c_o is the average concentration of the denser component and Δc is the concentration variation between top and bottom surfaces of the sample container.

Fluid properties like concentration and temperature can be described by locally averaged values (concentration and temperature profiles that can also change as a function of time) plus fluctuating quantities, $T(\mathbf{x},t) = T_o(\mathbf{x},t) + \delta T(\mathbf{x},t)$, or $c(\mathbf{x},t) = c_o(\mathbf{x},t) + \delta c(\mathbf{x},t)$. It has been demonstrated since a couple of decades that these fluctuations are long-ranged whenever the system is either in equilibrium and close enough to critical conditions or in non-equilibrium (NE) conditions [2,3]. The behavior of NE fluctuations is typically diffusive in the absence of gravity and in the fluid bulk. Recently it was also shown that diffusive fronts are self-affine, but not fractal [4]. Moreover, an increasing interest for studying fluctuations in situations that are not easily taken into account by available theories is arising [5].

If gravity is included in the system then it systematically influences the NE fluctuations for wave numbers smaller that a typical value $q < q_T^*$, where $(q_T^* L)^4 = Ra_T$ for temperature fluctuations or $q < q_s^*$, where $(q_s^* L)^4 = Ra_s$ for concentration fluctuations and $q = 2\pi/\lambda$ is the inverse of the fluctuation wavelength λ. Here Ra_s is a solutal Rayleigh number $Ra_s = \beta_c \mathbf{g} \cdot \boldsymbol{\nabla} c L^4/(\nu D)$, $\beta_c = \rho^{-1}(\partial\rho/\partial c)$ is the solutal expansion coefficient, Δc the concentration difference between the top and bottom of the sample and D is the mass diffusion coefficient. If boundary conditions are also considered, a *confinement* effect can be detected for fluctuations of lateral size that becomes comparable with the vertical thickness of the fluid layer. This has been experimentally shown only recently in

* Contribution to the Topical Issue "Non-isothermal transport in complex fluids", edited by Rafael Delgado-Buscalioni, Mohamed Khayet, José María Ortiz de Zárate and Fabrizio Croccolo.

[a] e-mail: fabrizio.croccolo@univ-pau.fr

combination with numerical and theoretical evidence [6,7]. In those papers the imposed thermal stress provided negative (stable) solutal Rayleigh numbers much larger than 1000 in modulus.

The Rayleigh number can be reduced by a factor of 10^6 by carrying out measurements in microgravity. On ground one may use density-matched samples, but it is difficult to obtain an effective matching in the presence of gradients, where matching works well at one temperature and concentration, but not at the others. The dependence of the Rayleigh number on the fourth power of the sample thickness suggests the interesting opportunity to greatly reduce the Rayleigh number by simply using thin samples. Varying the thickness by a factor of 30 is then equivalent to reduce gravity by a factor of $30^4 \approx 10^6$, resulting in conditions similar to those of microgravity.

In the present paper we adopt the latter scheme and focus our attention to the case of Rayleigh numbers smaller than 1000 in modulus and investigate both negative (stable) and positive (unstable) values. We set the modulus of the Rayleigh number by changing the thickness of the fluid layer in the range from $100\,\mu$m to $230\,\mu$m for an applied temperature difference of 10 K resulting in solutal Rayleigh numbers from about ± 50 up to about ± 700. We aim at understanding how the confinement affects the gravitational acceleration of larger fluctuations and to what extent an experiment on a thin layer of fluid can be considered equivalent to an experiment performed in microgravity conditions, where the solutal Rayleigh number is nominally zero.

2 Materials and methods

The investigated sample is a binary liquid mixture of Tetraline and *n*-Dodecane with mass fraction of 50.0%. Thermo-physical properties of the mixture are detailed in [6, 7]. To investigate the behavior of NE fluctuations we optically access the sample in the vertical direction. In order to achieve this, the sample is sandwiched between two sapphire windows of $40 \times 40 \times 8\,\mathrm{mm}^3$. The configuration of the cell is similar to the one utilized in previous experiments [6–10]. The large thermal conductivity of sapphire (about $35\,\mathrm{W/(mK)}$) allows using the windows both for allowing optical access to the cell and for thermalizing the liquid. The sample fluid is horizonthally contained by means of different plastic sheets with a hole of about 20 mm diameter. Each sapphire window is externally in contact with an annular thermoelectric device with an inner hole of diameter 13 mm. Each thermoelectric device is controlled by a Proportional-Integral-Derivative servocontrol and can transfer heat from/to a water circulation bath at constant temperature. The RMS stability of the average temperature and of the temperature difference applied to the sample is of the order of 1 mK/24 hours. The uniformity of the temperature gradient across the observation window is better than 5%. The cell assembly is supported by a kinematic table pneumatically isolated from the floor in order to reduce vibrations.

The optical technique of choice is shadowgraphy [11–13]. The layout of the setup is similar to that used in precedent experiments [8–10]. The light source is a superluminous diode (Super Lumen, SLD-MS-261-MP2-SM) $\lambda = 675 \pm 13\,\mathrm{nm}$ and a maximum intensity of about 5 mW coupled to a monomode optical fiber. The divergent beam coming out of the fiber is collimated by an achromatic doublet with a focal length of 150 mm. The large focal length of the doublet allows to achieve a uniform illumination of the sample. The collimated beam crosses the sample in the vertical direction and impinges onto a Charged Coupled Device (CCD) detector (AVT, PIKE-F421B) with a resolution of 2048×2048 pixels from which we crop images of 768×768 pixels. Each pixel has a real size of $7.4 \times 7.4\,\mu\mathrm{m}^2$ and a resolution of 14 bit.

A typical measurement sequence involves the sudden imposition of a temperature difference to the sample. A quasi-linear temperature profile establishes in the cell with a time constant of $\tau_{\mathrm{th}} = L^2/\kappa$, where L is the vertical thickness of the sample. In the case studied here $\kappa = 9.7 \times 10^{-4}\,\mathrm{cm^2\,s^{-1}}$ so that for example with the larger thickness of this study $L = 230\,\mu$m we obtain a thermal time constant of $\tau_{\mathrm{th}} = 0.55\,\mathrm{s}$. We can therefore consider that the thermal profile is well established after about 1 s. The concentration profile is considerably slower to establish due to the large Lewis number of the liquid binary mixture, here $Le = \kappa/D = 156$. In this case the solutal time constant is then $\tau_s = L^2/D$ and using the mass diffusion coefficient of the investigated sample $D = 6.2 \times 10^{-6}\,\mathrm{cm^2\,s^{-1}}$ one obtains $\tau_s = 85\,\mathrm{s}$, therefore to get a well-established concentration gradient one should wait less than 2 minutes. After the establishment of the concentration gradient a number $N = 20000$ images are acquired at the minimum available delay time of $\mathrm{d}t = 35\,\mathrm{ms}$. The series of images is further analyzed in subsets of 2000 images and the resulting structure functions are eventually averaged over the 10 available samples.

3 Results and discussion

In order to investigate NE fluctuations we make use of the Differential Dynamic Algorithm (DDA) combined with the Shadowgraph optical technique [8, 14–17]. Details of the procedure are provided in the cited papers. Here we report a sample of the acquired images, a difference image showing the fluctuations and the power spectrum of the difference image in order to evaluate the quality of the signal. The three of them are reported in fig. 1.

The acquired images are then utilized for computing the structure function of the system for all the measured wave vectors and for all the time delays. A sample of the obtained structure functions is shown in fig. 2 both as a function of the wave number q and the time delay Δt. Calculating the structure function out of a large number of images involves a hard computational load, therefore we make use of specific accelerated software running on Graphic Processing Unit [18].

In order to investigate the dynamics and the statics of NE fluctuations, the structure function $C_m(q, \Delta t)$ data

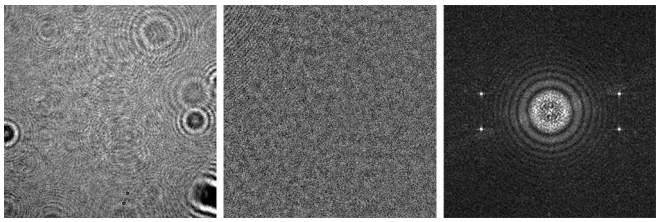

Fig. 1. Shadowgraph image of NE fluctuations for $L = 230\,\mu$m and $\Delta T = -10\,$K. (a) Sample image; the side corresponding to 5.7 mm, (b) image difference with a time delay of 3.5 s and (c) power spectrum of (b).

are fitted for each wave number through

$$C_m(q,\Delta t) = 2S(q)T(q)[1 - f(q,\Delta t)] + B(q), \qquad (1)$$

where $S(q)$ is the system static power spectrum, $T(q)$ is the optical technique transfer function, $f(q,\Delta t)$ the intermediate scattering function (ISF) and $B(q)$ a background noise. We also note that all along this paper we intend that the wave number q is the modulus of the wave vector $\boldsymbol{q}$ that almost identifies with its projection in the plane perpendicular to the temperature and concentration gradients: $\boldsymbol{q} \cong \boldsymbol{q}_\perp$.

The ISF is modeled here with a double exponential decay taking into account both temperature and concentration fluctuations, so that we can write it as

$$f(q,\Delta t) = a_1 \exp\left[-\frac{\Delta t}{\tau_1(q)}\right] + (1-a_1)\exp\left[-\frac{\Delta t}{\tau_2(q)}\right], \qquad (2)$$

where a_1 is the relative amplitude of the slowest mode and $\tau_1(q)$ and $\tau_2(q)$ are the slow and the fast mode time decays, respectively. Given the frame rate of our CCD camera of about 30 Hz, temperature fluctuations are detectable in a limited wave vector range. In the present paper we are interested only in concentration fluctuations and we will describe only the results of the slowest mode related to the latter contribution. Hence, we would like to stress that from fitting our data through eqs. (1) and (2) one obtains the following terms:

1) $a_1(q)$, $\tau_i(q)$, that is the relative amplitude of the slowest mode as well as the different time decays describing the dynamics of the system;
2) $S(q)T(q)$, that is the product of the total static power spectrum and the shadowgraph transfer function;
3) $B(q)$, the background of the system including also all the signals decaying faster than the acquisition rate of the camera.

In the following sections we will describe the resulting dynamics and statics obtained by the described procedure.

3.1 Time constant of NE fluctuations

As stated, the dynamics of NE fluctuations can be characterized in terms of the ISF (or equivalently normalized time correlation function) $f(q,\Delta t)$, with $f(q,0) = 1$. As anticipated, data have been fitted with the double exponential decay of eq. (2), but for most of the investigated

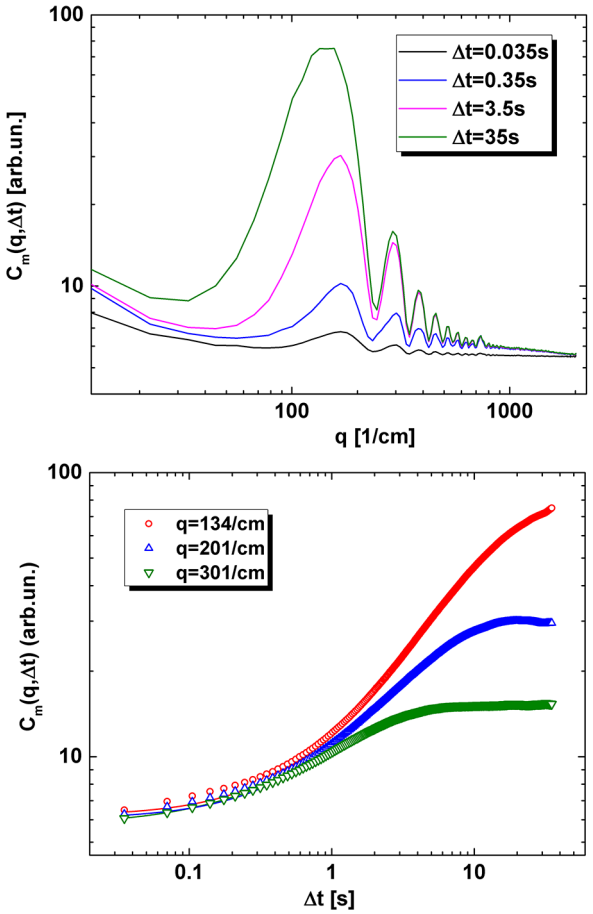

Fig. 2. Structure function $C_m(q,\Delta t)$ of NE fluctuations for $L = 230\,\mu$m and $\Delta T = -10\,$K as a function of the wave number q, for different delay times Δt (top) and the delay times Δt for different wave numbers q (bottom). Solid lines show fitting functions as explained in the text.

wave numbers the relative amplitude of the slowest mode a_1 is essentially one, thus reducing to a simple exponential decay. For very small wave numbers the two decays are observable and we will use in the following only the data related to the slow mode. Using a single exponential is good enough for wave numbers larger than about 50/cm, but introduces significant errors for smaller wave numbers, which justifies the adopted procedure.

Available theories accounting for the simultaneous presence of diffusion and gravity [19,20] and for the fluid bulk, *i.e.* far enough from the boundaries, predict different behaviors for the decay times of small-scale and large-scale fluctuations. In the fluid bulk the time decays are then well expressed by the equation

$$\left.\frac{\tau(\tilde{q})}{\tau_s}\right|_{d+g} = \frac{1}{\tilde{q}^2\left(1 - \frac{Ra_s}{\tilde{q}^4}\right)}, \qquad (3)$$

where $\tilde{q} = qL$ is the dimensionless wave number. This suggests that the fluctuation decay time has a clear maximum at the solutal characteristic wave vector $\tilde{q}_s^* =$

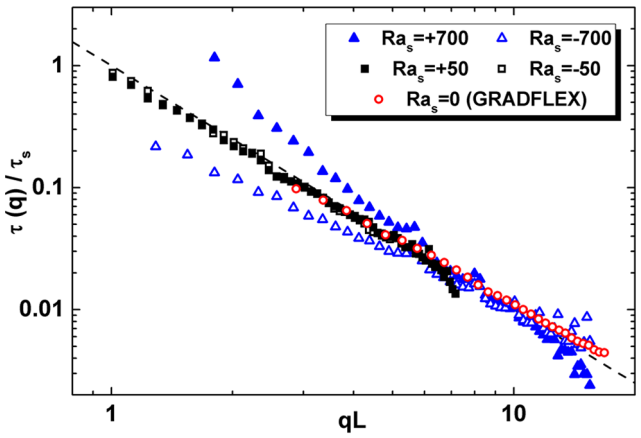

Fig. 3. Normalized time constants $\tau(q)/\tau_s$ at different positive and negative solutal Rayleigh numbers. Symbols stand for different experimental data as explained in the figure legend, while the dashed line stands for $\tau(q)/\tau_s = 1/\tilde{q}^2$.

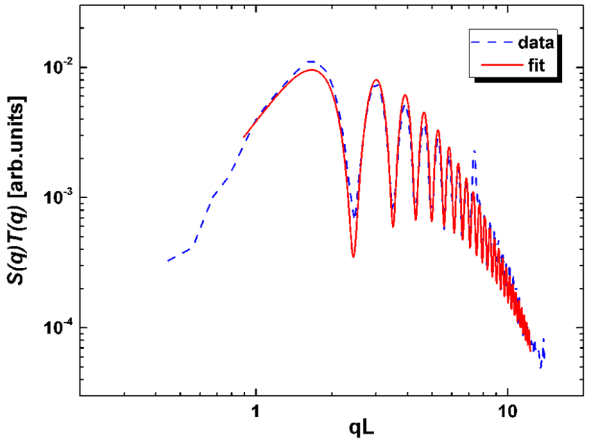

Fig. 4. Static power spectrum of concentration non-equilibrium fluctuations $a_1(q)S(q)T(q)$ for the solutal Rayleigh number $Ra_s = +50$.

$|Ra_s|^{1/4}$, which identifies the most persistent fluctuation in the system bulk. The behavior predicted by eq. (3) has been experimentally verified in a number of experiments [8, 14–16, 21, 22]. Note that eq. (3) implies that fluctuations of larger length scale decay faster, which is a non-intuitive result [16].

It was recently shown that the effect of confinement is that of slowing-down fluctuations of wave number smaller than $qL < \tilde{q}_b = \sqrt[4]{Ra_{s,\mathrm{cr}}} \cong 5.2$ [6, 7]. Hence, for the present paper we must consider that for small wave numbers the decay times are mainly due to confinement by

$$\left.\frac{\tau(\tilde{q}\to 0)}{\tau_s}\right|_c = \frac{1}{\tilde{q}^2\left(1-\frac{Ra_s}{Ra_{s,\mathrm{cr}}}\right)}\,. \tag{4}$$

Equation (4) is actually valid for any value of the solutal Rayleigh number $Ra_s < Ra_{s,\mathrm{cr}} = 720$ thus being valid also for small positive values of the solutal Rayleigh number below the threshold for solutal convection. For that reason we decided to investigate both positive and negative solutal Rayleigh number approximately smaller (in modulus) than 1000.

In fig. 3 we report the obtained time decays of NE concentration fluctuations obtained for different solutal Rayleigh numbers both negative (stabilizing thermal gradient) and positive (de-stabilizing thermal gradient). The main features visible in fig. 3 are the following:

1) No maximum can be detected in the time decays for the investigated negative and positive solutal Rayleigh numbers.
2) For dimensionless wave numbers qL smaller than about 5.2 the time decays are decreased (increased) by the effect of confinement for negative (positive) Rayleigh numbers.
3) The behavior of time decays becomes more and more similar to the pure diffusive one both for negative and positive solutal Rayleigh numbers, as far as the modulus of the Rayleigh number is decreased.

The latest point suggests that a strong confinement is rather similar to reducing gravity, which is mirrored by the expression of the solutal Rayleigh number depending also on the value of the gravity force acting on the system.

3.2 Static power spectrum

As stated in sect. 3 the DDA analysis provides also the intensity of the fluctuations multiplied by the optical transfer function, whose result is displayed in fig. 4 as a dashed blue line for the case of solutal Rayleigh number $Ra_s = +50$. Actually the data points are the product of $a_1(q)S(q)T(q)$, but, as stated above, they essentially coincide with $S(q)T(q)$ for most of the wave number range.

The optical layout utilized for the reported experiments is that of the shadowgraph, whose optical transfer function is an oscillatory function of the wave number q [12, 13], clearly observable in fig. 4. While it is outside the scope of the present paper to go into the refined details of the physical optics involved in the shadowgraph, we would like to recall here its basic equation well describing the oscillatory behavior [12, 13]

$$T(q) = \sin^2\left(\frac{q^2 z}{2k_o}\right), \tag{5}$$

where z is the distance between the sample plane and the plane imaged onto the sensor and k_o is the wave number of the light source in vacuum. In our case, without any lens between the sample cell and the sensor, z corresponds to the geometrical distance between the sample plane (its center) and the sensor. This equation is valid for a monochromatic light source with longitudinal coherence larger than the sample thickness L and for $z \ll k_o d/(2q)$, where d is the sample diameter [13]. As can be appreciated in fig. 4 the oscillations of the transfer function fade away for large wave numbers. This behavior can modeled by using a phenomenological equation that was proposed

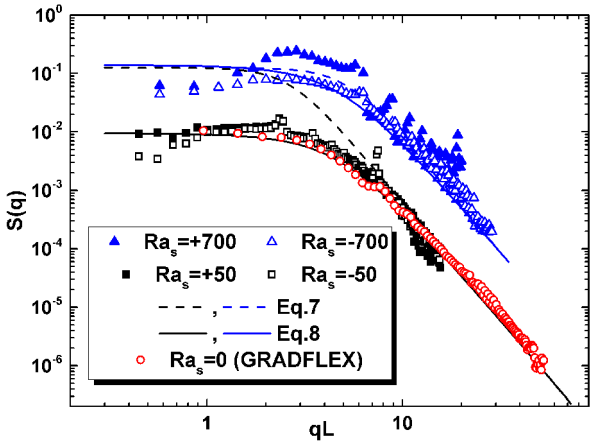

Fig. 5. De-convolved static power spectra $S(q)$ at different positive and negative solutal Rayleigh numbers. Different theoretical predictions are also included as detailed in the text. Dashed lines represent eq. (7), while solid lines represent eq. (8). Blue color is for $|Ra_s| = 700$, while black color is for $|Ra_s| = 50$. Red datapoints are for the microgravity GRADFLEX experiment [28–31].

in a precedent paper [9]

$$T(q) = 1/2 + \left[\sin^2\left(\frac{q^2 z}{2k_o}\right) - 1/2\right] \cdot e^{-q/q_x}, \qquad (6)$$

where the fit parameter q_x describes the speed at which the oscillations fade away. Provided that the shadowgraph transfer function can be finely evaluated, it is then tempting to deconvolve the static data to investigate the effect of confinement on the statics. In order to do that we first fit the data reported in fig. 4 by using eq. (6) multiplied by a standard equation for the power spectrum of concentration NE fluctuations not including the confinement [23,24]

$$S(\tilde{q}) = \frac{S_o}{1 - \frac{\tilde{q}^4}{Ra_s}}. \qquad (7)$$

The result of such fitting is also shown in fig. 4 as a continuous red line. No physical meaning is given to the resulting S_o and Ra_s obtained by the fitting at this stage. Only, the numerical values of z and q_x are used to get an experimental transfer function and the static data are finally divided in order to get the pure static signal $S(q)$ for different experimental conditions. This result is shown in fig. 5 for the investigated negative and positive Rayleigh numbers.

Datapoints are complemented with two different theoretical predictions. First, the solid lines correspond to the exact analytical expression recently provided in ref. [25] for microgravity conditions, or $Ra_s = 0$

$$S(\tilde{q}) = \frac{S'_o}{\tilde{q}^4}\left[1 + \frac{4(1-\cosh\tilde{q})}{\tilde{q}(\tilde{q}+\sinh\tilde{q})}\right]. \qquad (8)$$

This equation includes the effect of confinement on the intensity (statics) of NE fluctuations, but not the effect of gravity. The two continuous lines correspond to fitting eq. (8) to the corresponding data in the wave number range where the q^{-4} behavior is observed letting S'_o as the only free parameter and using the two different sample thicknesses of 100 μm and 230 μm.

Second, the dashed lines represent fitting eq. (7) to the corresponding data again in the wave number range where the q^{-4} behavior is observed letting S_o as the only free parameter and using the two different solutal Rayleigh numbers of -50 and -700. In this case only negative Rayleigh numbers are taken into account. It is worth pointing out once more that the latter equation takes into account diffusion and gravity, but not the confinement. Not surprisingly, the outcome of the fitting procedure provides almost identical values for S_o as, for a light scattering experiment, it depends on the temperature gradient multiplied by the sample thickness, therefore, finally on the applied temperature difference that is the same for the two experiments.

Clearly for the smaller absolute value of the solutal Rayleigh number of about $|Ra_s| = 50$ the predictions of eq. (8) including confinement, but not gravity, are much better than those of eq. (7) not including confinement. The data are worst described by the available theories for the case of the larger absolute values of the solutal Rayleigh number. In fact while both theories do fit pretty well the experimental data for large wave numbers where both gravity and confinement are negligible, they both fail for smaller wave numbers. In particular none of them is taking into account the different modulus of the solutal Rayleigh number thus not being able to describe the increase of the static power spectrum for dimensionless wave numbers qL around 5. This enhancement was previously shown in numerical calculations of the static power spectrum, as can be appreciated in fig. 2 of ref. [26]. Experimentally, a peak in the intensity of solutal fluctuations was also previously reported for a suspension of highly thermophilic nano-particles heated from above [27].

3.3 Discussion

In figs. 3 and 5 we included also data resulting from the micro-gravity experiment GRADFLEX. In the cited experiment concentration NE fluctuations were investigated for a binary mixture of Polystyrene and Toluene stressed by a temperature gradient. The GRADFLEX experiment was flown in 2007 on-board the Russian satellite FOTON M3. Relevant details can be found in the literature [28–31].

The comparison among our ground-based data and those obtained in micro-gravity allows fully appreciating the effect of the confinement both on the dynamics and the statics. In fact, in fig. 3 one can see that the time decays for $Ra_s = \pm 50$ obtained on Earth are quite similar to those obtained in micro-gravity. A similar result is obtained by analyzing fig. 5 where the GRADFLEX data are quite well superposed to our data. The dynamic data reported in fig. 3 are naturally normalized as we report normalized time constants $\tau(q)/\tau_s$, while the static data in fig. 5 are normalized so that the data in the large wave number range fit to the data for $Ra_s = \pm 50$.

As a concluding remark we would like to point out that the power spectra shown in fig. 5 present a slight dip for the smaller wave vector range $qL < 2$. This can be a signature of the fact that the stationary state was maybe not fully achieved when the experiment was performed. In the investigated situation of strong confinement it is possible that the solutal time constant τ_s computed out of the cell height L is not sufficient for reaching the steady state. Observing fig. 3, in fact, one can note that time constants for the smaller wave numbers normalized by τ_s can exceed unit for the investigated range of wave numbers. The dip observable in the statics is compatible with a similar behavior observed in the transient state of micro-gravity data, see ref. [30].

4 Conclusions

We have performed shadowgraph experiments to investigate the dynamics and the statics of NE concentration fluctuations by imposing a thermal stress to thin layers of a binary mixture in normal gravity conditions. We have applied positive and negative temperature gradients to observe the different effect of the confinement in the two cases and we have limited the temperature difference in order to keep the solutal Rayleigh number smaller than the critical value for convection.

DDA has been applied to the acquired images providing the structure function $C_m(q, \Delta t)$ of NE fluctuations and ultimately both the time decay of concentration NE fluctuations and their intensity. The time decays show clear evidence of the confinement, because the effect of gravity on small wave number fluctuations is almost not detectable. Time decays for smaller (in modulus) solutal Rayleigh numbers are essentially identical to the values obtained in micro-gravity conditions.

The analysis of the statics required the evaluation of the Shadowgraph transfer function. After deconvolution of the latter, static data revealed once again that confinement effects wash out the effect of gravity, thus making data for solutal Rayleigh number of ± 50 comparable to those obtained through the GRADFLEX experiment.

We suggest that this approach may be utilized for performing preliminary experiments on ground in preparation to micro-gravity activities.

As a final remark we stress the fact that available theories are not capable of describing the combined effect of gravity and confinement on the intensity of the concentration non-equilibrium fluctuations. The relative maximum obtained in the power spectrum for $Ra_s = 700$ is similar to previous theoretical results obtained by full Galerkin approximations including also temperature fluctuations. This suggests that an additional element to take into account in the theory is the coupling between concentration and temperature fluctuations.

We kindly thank support from the SCCO Space Project (a joint venture of ESA and the Chinese Space Agency). FC acknowledges financial support from the Centre National d'Etudes Spatiales of France. The GRADFLEX team as well as ESA and NASA are acknowledged for providing the data in micro-gravity conditions. FC acknowledges fruitful discussions with Alberto Vailati and Doriano Brogioli.

References

1. A. Ryskin, H.W. Müller, H. Pleiner, Phys. Rev. E **67**, 046302 (2003).
2. J.M. Ortiz de Zárate, J.V. Sengers, *Hydrodynamic Fluctuations in Fluids and Fluid Mixtures* (Elsevier, Amsterdam, 2006).
3. F. Croccolo, J.M. Ortiz de Zárate, J.V. Sengers, Eur. Phys. J. E. **39**, 125 (2016).
4. D. Brogioli, F. Croccolo, A. Vailati, Phys. Rev. E **94**, 022142 (2016).
5. P. Baaske, H. Bataller, M. Braibanti, M. Carpineti, R. Cerbino, F. Croccolo, A. Donev, W. Köhler, J.M. Ortiz de Zárate, A. Vailati, Eur. Phys. J. E **39**, 119 (2016).
6. C. Giraudet, H. Bataller, Y. Sun, A. Donev, J.M. Ortiz de Zárate, F. Croccolo, Europhys. Lett. **111**, 60013 (2015).
7. C. Giraudet, H. Bataller, Y. Sun, A. Donev, J.M. Ortiz de Zárate, F. Croccolo, Eur. Phys. J. E **39**, 120 (2016).
8. F. Croccolo, H. Bataller, F. Scheffold, J. Chem. Phys. **137**, 234202 (2012).
9. F. Croccolo, F. Scheffold, H. Bataller, C. R. Méc. **341**, 378 (2013).
10. F. Croccolo, F. Scheffold, A. Vailati, Phys. Rev. Lett. **111**, 014502 (2013).
11. G.S. Settles, *Schlieren and Shadowgraph Techniques* (Springer, Berlin, 2001).
12. S. Trainoff, D.S. Cannell, Phys. Fluids **14**, 1340 (2002).
13. F. Croccolo, D. Brogioli, Appl. Opt. **50**, 3419 (2011).
14. F. Croccolo, D. Brogioli, A. Vailati, M. Giglio, D.S. Cannell, Appl. Opt. **45**, 2166 (2006).
15. F. Croccolo, D. Brogioli, A. Vailati, M. Giglio, D.S. Cannell, Ann. N.Y. Acad. Sci. **1077**, 365 (2006).
16. F. Croccolo, D. Brogioli, A. Vailati, M. Giglio, D.S. Cannell, Phys. Rev. E **76**, 041112 (2007).
17. R. Cerbino, V. Trappe, Phys. Rev. Lett. **100**, 188102 (2008).
18. G. Cerchiari, F. Croccolo, F. Cardinaux, F. Scheffold, Rev. Sci. Instrum. **83**, 106101 (2012).
19. P.N. Segrè, R. Schmitz, J.V. Sengers, Physica A **195**, 31 (1993).
20. P.N. Segrè, J.V. Sengers, Physica A **198**, 46 (1993).
21. F. Croccolo, H. Bataller, F. Scheffold, Eur. Phys. J. E **37**, 105 (2014).
22. C. Giraudet, H. Bataller, F. Croccolo, Eur. Phys. J. E **37**, 107 (2014).
23. A. Vailati, M. Giglio, Nature **390**, 262 (1997).
24. A. Vailati, M. Giglio, Phys. Rev. E **58**, 4361 (1998).
25. J.M. Ortiz de Zárate, T.R. Kirkpatrick, J.V. Sengers, Eur. Phys. J. E **38**, 99 (2015).
26. J.M. Ortiz de Zárate, F. Peluso, J.V. Sengers, Eur. Phys. J. E **15**, 319 (2004).
27. F. Giavazzi, A. Vailati, Phys. Rev. E **80**, 015303(R) (2009).
28. A. Vailati, R. Cerbino, S. Mazzoni, C.J. Takacs, D.S. Cannell, M. Giglio, Nat. Commun. **2**, 290 (2011).
29. C.J. Takacs, A. Vailati, R. Cerbino, S. Mazzoni, M. Giglio, D.S. Cannell, Phys. Rev. Lett. **106**, 244502 (2011).
30. R. Cerbino, Y. Sun, A. Donev, A. Vailati, Sci. Rep. **5**, 14486 (2015).
31. F. Croccolo, C. Giraudet, H. Bataller, R. Cerbino, A. Vailati, Micrograv. Sci. Technol. **28**, 467 (2016).